Acid ceramidase controls proteasome inhibitor resistance and is a novel therapeutic target for the treatment of relapsed/refractory multiple myeloma

Ryan T. Bishop,[1] Tao Li,[1] Praneeth R. Sudalagunta,[2] Mostafa M. Nasr,[1,3] Karl J. Nyman,[1,3] Raghunandan R. Alugubelli,[4] Mark B. Meads,[1,5] Jeremy S. Frieling,[1] Niveditha Nerlakanti,[1,3] Marilena Tauro,[1] Bin Fang,[6] Steven Grant,[7] John M. Koomen,[6,8] Ariosto S. Silva,[2] Kenneth H. Shain[1,5] and Conor C. Lynch[1]

[1]Department of Tumor Metastasis and Microenvironment, H. Lee Moffitt Cancer Center and Research Institute, Tampa, FL; [2]Department of Metabolism and Physiology, H. Lee Moffitt Cancer Center and Research Institute, Tampa, FL; [3]Cancer Biology Ph.D. Program, University of South Florida, Tampa, FL; [4]Collaborative Data Services Core, H. Lee Moffitt Cancer Center and Research Institute, Tampa, FL; [5]Department of Malignant Hematology, H. Lee Moffitt Cancer Center and Research Institute, Tampa, FL; [6]Molecular Medicine, H. Lee Moffitt Cancer Center and Research Institute, Tampa, FL; [7]Virginia Commonwealth University (VCU) Massey Cancer Center Richmond, VA and [8]Department of Molecular Oncology, H. Lee Moffitt Cancer Center and Research Institute, Tampa, FL, USA

Correspondence: C.C. Lynch
conor.lynch@moffitt.org

Received: April 23, 2024.
Accepted: November 27, 2024.
Early view: December 5, 2024.

https://doi.org/10.3324/haematol.2024.285587

Abstract

Multiple myeloma (MM) patients are often refractory to targeted therapies including proteasome inhibitors. Here, analysis of RNA sequencing data derived from 672 patients with newly diagnosed or relapsed/refractory disease identified the acid ceramidase, ASAH1, as a key regulator of resistance to proteasome inhibitors. Genetic or pharmacological blockade of ASAH1 remarkably restored sensitivity to proteasome inhibitors and protected mice from resistant MM progression *in vivo*. Mechanistically, ASAH1 depletion of ceramide promoted SET inhibition of PP2A phosphatase activity, thus facilitating increased expression and activity of the pro-survival proteins, MCL-1 and BCL-2. We corroborated these findings in human MM datasets, and in *ex vivo* patients' MM cells. These preclinical studies suggest that ASAH1 may be a potential therapeutic target for the treatment of relapsed/refractory MM.

Introduction

Multiple myeloma (MM) is a clonal plasma cell malignancy in which the colonization and expansion of malignant clones in the bone marrow results in osteolysis, hypercalcemia, renal insufficiency, anemia and immunosuppression.[1,2] Preclinical and clinical studies into the defining genetic and molecular alterations that drive MM pathophysiology, such as bone marrow microenvironment and ubiquitin-proteasome system dependency, have led to the development of numerous therapies to target MM-specific vulnerabilities. In particular, the introduction of proteasome inhibitors (PI), such as bortezomib and carfilzomib, immunomodulatory drugs, and, more recently, selective inhibitors of nuclear export, and cellular and non-cellular immunotherapies has significantly enhanced survival rates of MM patients.[3] However, MM remains incurable, and relapsed/refractory MM (RRMM), defined primarily as progressive disease on treatment within 60 days of a given therapy,[4,5] occurs frequently leading to the patient's demise. Thus, identifying the mechanisms governing resistance can facilitate the search for effective therapies for the treatment of RRMM. Alterations in the cellular and molecular composition of the MM microenvironment as well as the development of acquired resistance mechanisms drive the evolution of RRMM. Typically, these mechanisms collectively enhance activation and/or expression of pathways essential to RRMM proliferation (e.g., RAS/MAPK, NFκB, PI3K/AKT, JAK/STAT, MYC)[6-9] and/or survival (e.g., BCL-2 family members; BCL-2, MCL-1, BCL-xL, BCL-w, and BFL-1).[10-12] Identification of resistance mechanisms can lead to the development of novel targeted therapies, an example being the recent Food and Drug Administration-approved BCL-2 inhibitor, venetoclax. However, elevated MCL-1 levels can lead to venetoclax resistance in MM.[13] Therefore, therapies that can target upstream processes that regulate these pathways

may exhibit superior efficacy or provide additional benefits when given in combination. In this regard, sphingolipid metabolism has been associated with increased pro-survival signaling which, in turn, has pathogenic implications for several malignancies including MM.[14]

Sphingolipid metabolism largely involves regulating the balance between intracellular ceramide levels and conversion of ceramide to products such as sphingosine 1-phosphate (S1-P). Ceramides are fatty acid chains that can vary in length through the addition of carbon moieties and are critical for cell viability. For example, accumulation of ceramides, specifically C2 or C6, induces cell cycle arrest in malignant cells, whereas increases in C16 or C18 promote autophagic and apoptotic cell death through JNK and PKC.[15,16] Notably, RRMM cells have significantly lower levels of ceramide compared to those from newly diagnosed drug-naïve patients.[17] In contrast, the ceramide product, S1-P is regarded as a pro-tumorigenic sphingolipid. S1-P is generated following ceramidase-mediated hydrolysis of ceramides into sphingosines, which are subsequently phosphorylated by sphingosine kinases types 1 and 2 (SPHK1/2).[18] S1-P has been shown to elicit pro-survival signaling through multiple effectors including, but not limited to, Myc and STAT3.[19-23]

Herein, we analyzed RNA-sequencing data from the Pentecost Myeloma Research Center (PMRC) at Moffitt derived from patients with newly diagnosed MM (NDMM), early relapsed/refractory MM (ERMM) and late relapsed/refractory MM (LRMM) and identified that increased expression of genes related to sphingolipid metabolism was significantly associated with relapsed/refractory disease. Specifically, this increase correlated with higher expression of the acid ceramidase, ASAH1, a hydrolase located in acidic lysosomes that converts pro-apoptotic ceramides into pro-survival S1-P. Notably, ASAH1 expression was found to be significantly upregulated in patients treated with any PI-containing regimen and predicted poorer overall survival when patients were treated with PI-containing regimens. Here, we delineate a causal role for ASAH1 in PI-resistance which has not previously been defined.

Methods

Patients' data

We investigated the expression of sphingolipid metabolism genes in cancer cells from 672 MM patients. Samples were taken from patients with NDMM before treatment (N=187), from patients with ERMM (i.e., who had received 1-3 prior lines of therapy, N=303) or from patients with LRMM, (who had received >3 prior lines of therapy, N=182). Investigators obtained signed informed consent from all patients who were enrolled in the clinical trials/protocols MCC14745, MCC14690, and MCC18608 conducted at the H. Lee Moffitt Cancer Center and Research Institute, as approved by the Institutional Review Board. To this end, patients' samples were used in accordance with the Declaration of Helsinki, International Ethical Guidelines for Biomedical Research Involving Human Subjects (CIOMS), Belmont Report, and U.S. Common Rule. The medical records were deidentified, and only the following clinically relevant information was reviewed: (i) patients' survival, (ii) the treatment administered (therapeutic agents, doses, and schedule) prior to biopsy, and (iii) cytogenetics. RNA-sequencing data were normalized by Z-score. Patients were considered resistant to a treatment if they had progressed on or within 90 days of a given treatment. PI resistance included resistance to bortezomib, carfilzomib, oprozomib or marizomib. Resistance to immunomodulatory drugs included resistance to thalidomide, lenalidomide or pomalidomide. Chemoresistance included resistance to combinations of etoposide, vincristine, doxorubicin, and cyclophosphamide. Anti-CD38 resistance included resistance to daratumumab or isatuximumab. All MM patients were clustered using clustergrammer (version 2.0) based on the expression of 30 genes (WP_Sphingolipid Metabolism) or SET/ASAH1/MCL1/BCL2. Kaplan-Meier survival analyses for clusters and individual genes was performed using Prism.

Animal studies

All animal experiments were done with the approval of the University of South Florida (Tampa, FL, USA) Institutional Animal Care and Use Committee (CCL; #7356R). Male and female 6-week-old immunodeficient NOD-SCIDγ (NSG) mice were divided into tumor-naïve or tumor-bearing mice (25/group). For the ceranib-2/bortezomib combination study, phosphatidylserine receptor (PSR) - red fluorescence protein (RFP) MM cells were injected ($5x10^6$ cells/100 μL phosphate-buffered saline) by tail vein inoculation. Tumors were allowed to establish and were grown until RFP detection (Perkin Elmer IVIS Lumina) in the long bones (day 28) and then the animals were divided into four groups. Mice were treated with either vehicle, an induction dose of ceranib-2 (50 mg/kg, 5xweek), bortezomib (0.5 mg/kg, 2xweek) or combination treatment. After 1 week, the ceranib-2 dose was dropped to a maintenance level (5 mg/kg, 5xweek). For the ASAH1-knockdown ($ASAH1^{KD}$) study, PSR-Control-RFP, PSR-$ASAH1^{KD}$-RFP cells ($5x10^6$ cells/100 μL phosphate-buffered saline) or phosphate-buffered saline (100 μL) were inoculated into the mice via tail vein injection. Bortezomib treatment (0.5 mg/kg, 2xweek) was initiated after detection of serum IgE (day 21) and followed clinical treatment schedules (2 weeks on/1 week off) until day 63 when the first mice reached the endpoint of hindlimb paralysis. The mice were then euthanized by CO_2 inhalation and cervical dislocation. Tibiae were excised and soft tissue removed for X-ray, histological and flow cytometric analyses.

Additional methodological details are provided in the *Online Supplementary Material*.

Results

Sphingolipid metabolism and ASAH1 are elevated in patients with relapsed/refractory multiple myeloma and predict clinical outcome in these patients

A number of oncogenic drivers of MM have been identified but recently there has been a shift towards understanding how metabolic processes can contribute to MM progression and resistance. Sphingolipid metabolism in particular has been associated with increased pro-survival signaling which, in turn, has pathogenic implications. Less is known regarding sphingolipid metabolism in RRMM. To fill this gap, we leveraged RNA-sequencing data from the PMRC at Moffitt, studying MM cells derived from patients with NDMM (treatment-naïve, N=187), ERMM (1-3 lines of therapy, N=303) and LRMM (>3 lines of therapy N=182). We next assessed the expression of 30 genes involved in sphingolipid metabolism across this dataset. (*Online Supplementary Figure S1A, B*, *Online Supplementary Table S1*). Our analyses revealed that sphingolipid metabolism genes have significantly higher expression in RRMM (Figure 1A). Hierarchical clustering analysis revealed two distinct clusters (Sphingo^{Low} and Sphingo^{High}), with the proportion of Sphingo^{High} patients increasing from NDMM to LRMM (*Online Supplementary Figure S2A*). Notably, Sphingo^{High} patients had significantly shorter overall survival compared to Sphingo^{Low} patients, and this was particularly evident in RRMM (ERMM and LRMM patients combined) (Figure 1B, *Online Supplementary Figure S2B*).

Ceramides are the central sphingolipids from which multiple sphingolipid species are derived (*Online Supplementary Figure S1B*). Our analysis revealed that ASAH1 expression was significantly higher in ERMM and LRMM patients than in patients with NDMM (Figure 1C). We also noted a reduction in total ceramides in drug-resistant MM cell lines compared to their drug-sensitive isogenic counterparts (Figure 1D) and increased levels of S1-P (Figure 1D), consistent with previously published reports.[17] These data indicate enhanced conversion of ceramide into S1-P in relapsed/refractory cells. Notably, of the enzymes involved in ceramide conversion to S1-P, only ASAH1 and sphingosine kinase-1 (SPHK1) were significantly upregulated in both ERMM and LRMM (*Online Supplementary Figure S2C*). We next examined whether these genes were associated with resistance to standard-of-care therapies. While SPHK1 showed no significant association with any particular standard-of-care therapy, ASAH1 was significantly enriched in RRMM patients who were resistant to any PI-containing regimen (Figure 1E). Of note, ASAH1 was not significantly associated with any cytogenetic risk groups (*Online Supplementary Figure S2D*). Furthermore, in the PMRC cohort, we found that high ASAH1 expression (>NDMM median Z-score) in relapsed/refractory patients (regardless of any prior treatment) correlated with a worse overall survival (>2-fold survival reduction) when those patients specifically received a PI-containing regimen were compared to those who did not (*Online Supplementary Figure S2E*). We further confirmed this correlation by interrogating patients' data from the Multiple Myeloma Research Foundation (MMRF) CoMMpass trial (NCT0145429 - IA16). Analyses showed that newly diagnosed patients expressing high levels of ASAH1 mRNA (ASAH1^{High}, N=385) had significantly shorter duration of response (503 days *vs*. 804 days), progression-free survival (1,053 *vs*. 1,397 days) and overall survival (2,183 days *vs*. not reached) compared to patients with low ASAH1 expression (ASAH1^{Low}, N=385) (*Online Supplementary Figure S2E*). Importantly, 73.6% of these patients received PI-based regimens as first-line therapy (*MMRIA16*). We further confirmed that established human PI-resistant MM cell lines[24-26] and a PI-resistant derivative of 5TGM1 (5TGM1-C300R) generated in-house exhibited elevated ASAH1 at the protein level in addition to elevated activity, as measured via the RBM14C12 assay, compared to their isogenic parental controls (Figure 1F, *Online Supplementary Figures S2G* and *S3*). Taken together, these data establish ASAH1 as potentially playing a key role in mediating PI-resistance specifically in RRMM.

ASAH1 is a potential therapeutic target in relapsed/refractory multiple myeloma

To determine whether ASAH1 was playing a causal role in promoting RRMM resistance, we first generated several ASAH1 knockdown PI-resistant MM cell lines using three independent shRNA constructs to reduce protein expression and subsequently activity down to levels comparable with those of PI-sensitive cells (*Online Supplementary Figure S4A, B*). The two most effective constructs (PSR ASAH1 KD1 and KD3) were chosen for downstream analyses. shRNA-mediated knockdown of ASAH1 expression in PI-resistant MM cell lines (*Online Supplementary Figure S4A, B*) led to a modest yet significant decrease in MM cell growth over 48-72 hours *in vitro* (Figure 2A, *Online Supplementary Figure S4C*). We then focused on the feasibility of pharmacological ASAH1 inhibition. Notably, several ASAH1-targeted inhibitors have been developed given the role of the ceramidase in non-malignant pathologies such as Alzheimer disease.[27-33] Of the available inhibitors, we found ceranib-2 to be the most effective (Figure 2B, *Online Supplementary Figure S4D*). Importantly, this inhibitor has also been characterized *in vivo*, showing no signs of overt toxicity,[31] so we moved forward with this reagent. Subsequently, we observed that ceranib-2 reduced PI-resistant cell survival to significantly lower levels compared to that of PI-sensitive cells using six independent isogenic cell line series (half maximal inhibitory concentration [IC_{50}] range of 0.6-5.5 μM *vs*. 0.2-1.6 μM for PI-sensitive or PI-resistant MM, respectively) after 72 hours of treatment (Figure 2C). To test whether pharmacological inhibition of ASAH1 with ceranib-2 was effective for the treatment of PI-resistant MM *in vivo*, PI-resistant PSR[25,26] expressing RFP (PSR^{RFP}) were injected via the tail vein into NSG mice. To better mimic late-stage disease, we allowed PSR^{RFP} cells to home to and colonize the bone and initiated treatments 30 days after inoculation, following detection of serum IgE (day 21)

and an RFP signal in the hindlimbs (day 28). At day 30, mice were divided into three groups and treated with vehicle, 5 mg/kg ceranib-2 five times a week[31] or 0.5 mg/kg bortezomib twice weekly (approximating the clinical schedule and dose of 1.3 mg/m^2). Longitudinal RFP imaging revealed ceranib-2 treatment significantly reduced growth of PI-resistant MM cells compared to vehicle and bortezomib-treated controls (Figure 2D, E), as evidenced by 34.5% and 38.4% reductions in total radiant efficiency at day 63 compared to the total radiant efficiency in vehicle- and bortezomib-treated mice,

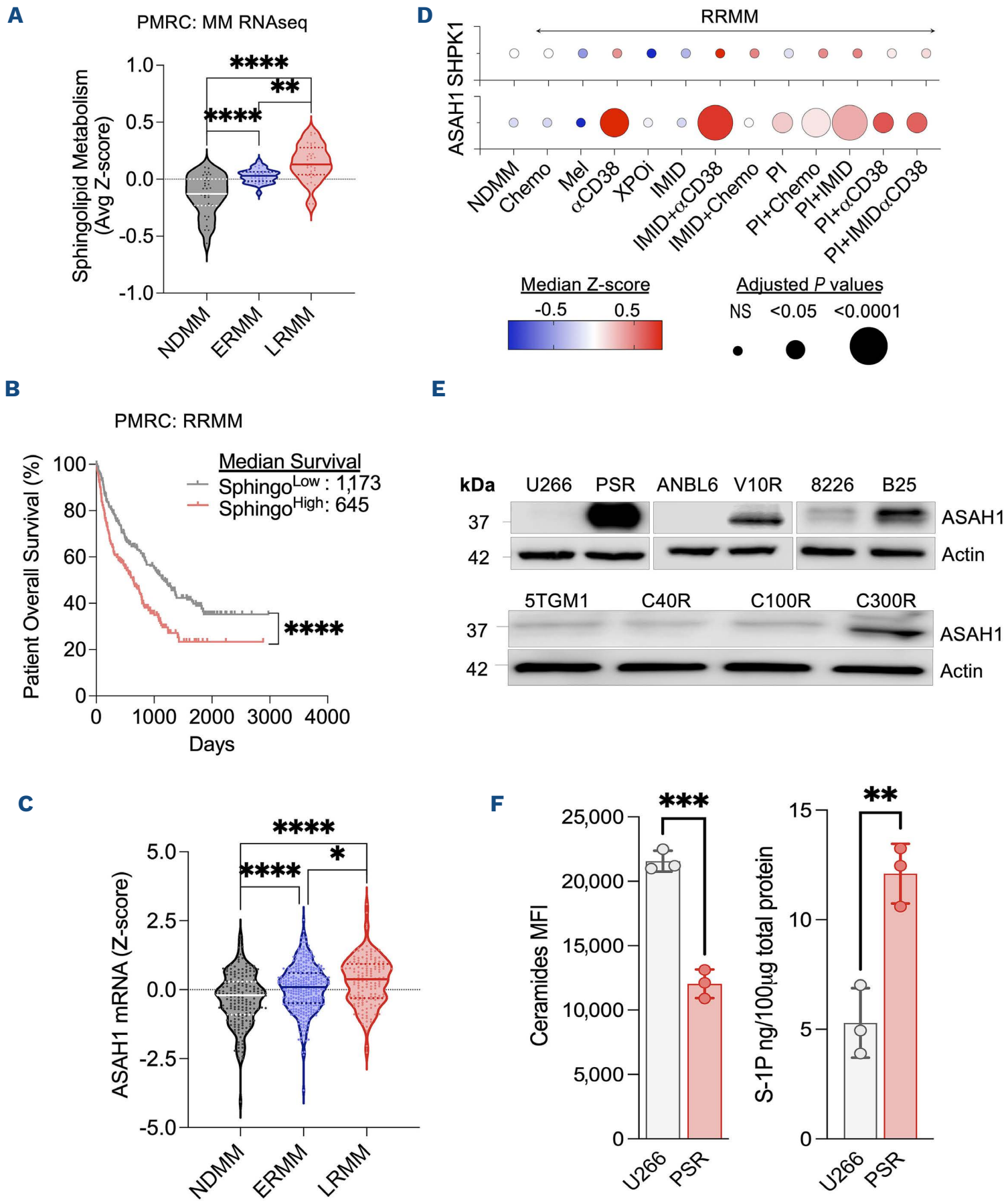

Figure 1. Sphingolipid metabolism and ASAH1 are elevated in proteasome inhibitor-resistant multiple myeloma. (A) RNA-sequencing was performed on the Pentecost Myeloma Research Center (PMRC) multiple myeloma (MM) cohort consisting of patients with newly diagnosed multiple myeloma (NDMM; 0 prior lines of therapy), early relapse multiple myeloma, (ERMM, 1-3 lines of prior therapy) and late relapse multiple myeloma (LRMM, >3 lines of prior therapy). The expression of 30 genes related to sphingolip-

Continued on following page.

id metabolism was assessed in NDMM (N=187), ERMM (N=303) and LRMM (N=182) patients. Each dot represents the median score for a gene. (B) MM patients were divided into groups based on the average expression of 30 sphingolipid genes (Sphingo^{Low} and Sphingo^{High}). Kaplan-Meier plots show the overall survival of ERMM and LRMM patients in Sphingo^{Low} (average Z-score <0, N=234) and Sphingo^{High} clusters (average Z-score >0, N=247). The inset indicates median survival in days. (C) The expression of ASAH1 mRNA was assessed in the PMRC MM cohort. The violin plot shows the median expression of ASAH1 mRNA in NDMM (N=187), ERMM (N=303) and LRMM (N=182) patients' samples. Dots represent individual patients. (D) The expression of ASAH1 mRNA was assessed in the PMRC MM cohort and patients were divided into NDMM and RRMM groups. The RRMM group was further subdivided based on the treatment regimen that each patient was given prior to relapse. The bubble blot shows the median ASAH1 expression (Z-score) in newly diagnosed, or myeloma patients resistant to each indicated treatment. Colored bubbles represent median Z-scores of each group. Bubble size represents the statistical significance between NDMM and resistance to treatment. (E) Whole cell lysates were prepared from isogeneic proteosome inhibitor (PI)-sensitive (U266, ANBL-6, 8226, 5TGM1) and PI-resistant (PSR, V10-R, B25, C40R, C100R, C300R) MM cell lines. The immunoblot shows the expression of ASAH1 and the loading control, actin, in each cell line. (F) The level of ceramide was assessed by flow cytometry in MM cell lines, U266 and their PI-resistant derivative. The bar chart indicates the quantified median fluorescence intensity of ceramide in each cell line (left). The level of sphingosine-1 phosphate (S1-P) was assessed by enzyme-linked immunosorbent assay in MM cell lines, U266 and their PI-resistant derivative, PSR. The bar chart shows the amount of intracellular S1-P in each cell line normalized to 100 μg of total protein (right). Values are mean ± standard deviation of three independent experiments. Statistical significance was derived by ordinary one-way analysis of variance with the Dunnett multiple comparisons test (A, C and D), log-rank (Mantel-Cox) test (B) and Student *t* test (F). **P*<0.05, ***P*<0.01, ****P*<0.001, *****P*<0.0001. Chemo: chemotherapy; Mel: melphalan; αCD38: antiCD38 antibody; XPOi: exportin 1 inhibitor; IMID: immunomodulatory drug; MFI: mean fluorescence intensity.

respectively (*Online Supplementary Figure S5A*). Similar results were obtained by *ex vivo* RFP fluorescence assisted cell sorting analysis (*Online Supplementary Figure S5B*), which demonstrated ceranib-2-treated mice had 42.53% and 58.14% reductions in the number of RFP MM cells in the bone marrow at endpoint, compared to the numbers in vehicle- and bortezomib-treated mice respectively. These reductions in tumor burden led to significant 1.25- and 1.17-fold increases in median overall survival time of the ceranib-2-treated mice compared to vehicle- and bortezomib-treated controls, respectively (Figure 2F). As expected, bortezomib treatment had no effect on overall survival in PI-resistant MM compared to that of vehicle-treated mice (Figure 2D, E).

Given the clinical significance of MM on bone destruction, we also examined the impact of ceranib-2 treatment on MM-induced bone disease and observed a significant reduction in cortical osteolytic lesions (*Online Supplementary Figure S6A*), trabecular bone destruction (*Online Supplementary Figure S6B, D*) and in the number of tartrate-resistant acid phosphatase (TRAcP)-positive osteoclasts (*Online Supplementary Figure S6C*) in ceranib-2-treated mice compared to those in vehicle-treated controls. Taken together, these data point to ASAH1 inhibition as a viable therapeutic target for the treatment of RRMM and the associated bone disease that leads to fractures and other complications in patients.

ASAH1 inhibition alters sphingolipid levels leading to loss of anti-apoptotic protein expression and activity

We next investigated the potential mechanisms through which ASAH1 might contribute to treatment resistance using gene-set enrichment analysis. ASAH1^{High} patients displayed upregulation of gene signatures involved in the metabolism of lipids and sphingolipids, as might be expected, and also regulation of apoptosis (Figure 3A). Studies have implicated ASAH1 and sphingolipid metabolism in the expression and activation of pro-survival proteins such as MCL-1 and BCL-2.[16,34] Independent analysis of the CoMMpass and PMRC datasets revealed that ASAH1^{High} patients had significantly increased levels of anti-apoptotic MCL-1 and BCL-2 mRNA (Figure 3B, *Online Supplementary Figure S7A*), with MCL-1, but not BCL-2 expression increasing in RRMM (*Online Supplementary Figure S7B*). Consistent with our patients' data thus far, we observed that PI-resistant MM cell lines have elevated levels of ASAH1, and increased levels of total and phosphorylated MCL-1/BCL-2 compared to parental PI-sensitive MM cell lines (Figure 3C, *Online Supplementary Figure S7C, D*). In ASAH1 knockdown cell lines, we also observed reduced expression of both the total and phosphorylated forms of MCL-1 and BCL-2. In agreement, we observed that treatment of PI-resistant MM with ceranib-2 reduced MCL-1 and BCL-2 protein levels (Figure 3D, *Online Supplementary Figure S8A, B*) combined with an induction of apoptosis (*Online Supplementary Figure S8C*).

Since ASAH1 has been reported to hydrolyze ceramides into sphingosine for conversion to S1-P by SPHK, we assessed the levels of ceramide and S1-P following ASAH1 inhibition. As expected, both ASAH1^{KD} and treatment with ceranib-2 enhanced levels of total ceramides in PI-resistant cells with a concurrent reduction in intracellular S1-P (Figure 3E). In *ex vivo* bone marrow supernatants derived from our *in vivo* studies (Figure 2), we also observed a complete loss of S1-P in ceranib-2-treated mice (Figure 3E).

To test whether loss of S-1P or the accumulation of ceramides was responsible for changes in anti-apoptotic protein levels, we treated PI-resistant MM cells with the SPHK1/2 inhibitor, SKI-178 and noted no effect on the levels of anti-apoptotic proteins (Figure 3F, *Online Supplementary Figure S8D*). However, addition of exogenous ceramide reduced both MCL-1 and BCL-2 levels in PI-resistant MM (Figure 3F, *Online Supplementary Figure S8D*). Taken together, our data indicate that ASAH1 controls PI-resistant cell viability

A

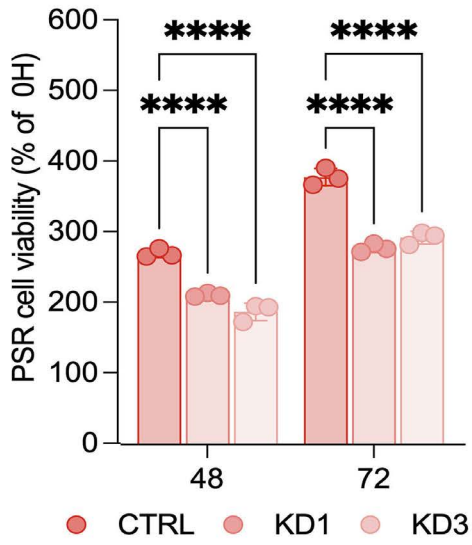

B

Inhibitor	ASAH1 IC_{50} (μM)	PSR IC_{50} (μM)
Ceranib-2	2.146	0.89
LCL-521	5.130	0.75
Carmofur	19.61	13.01
ARN-14998	NR	86.37
ARN-14974	NR	346.1

C

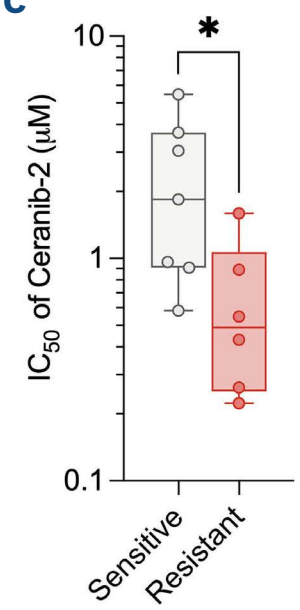

D

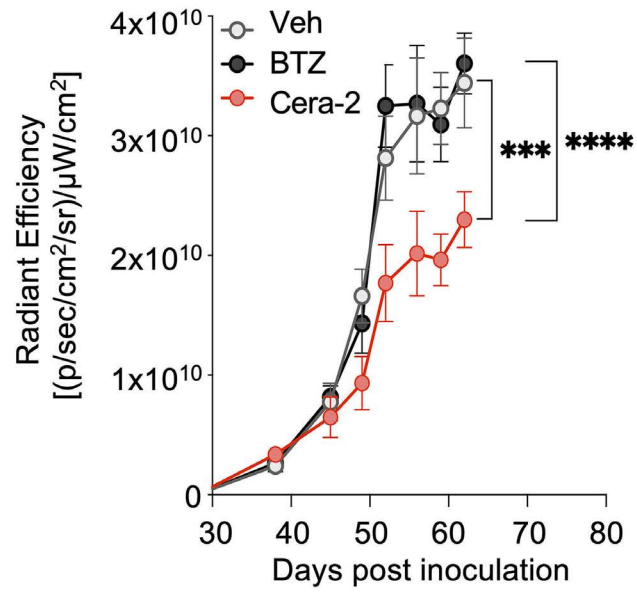

E

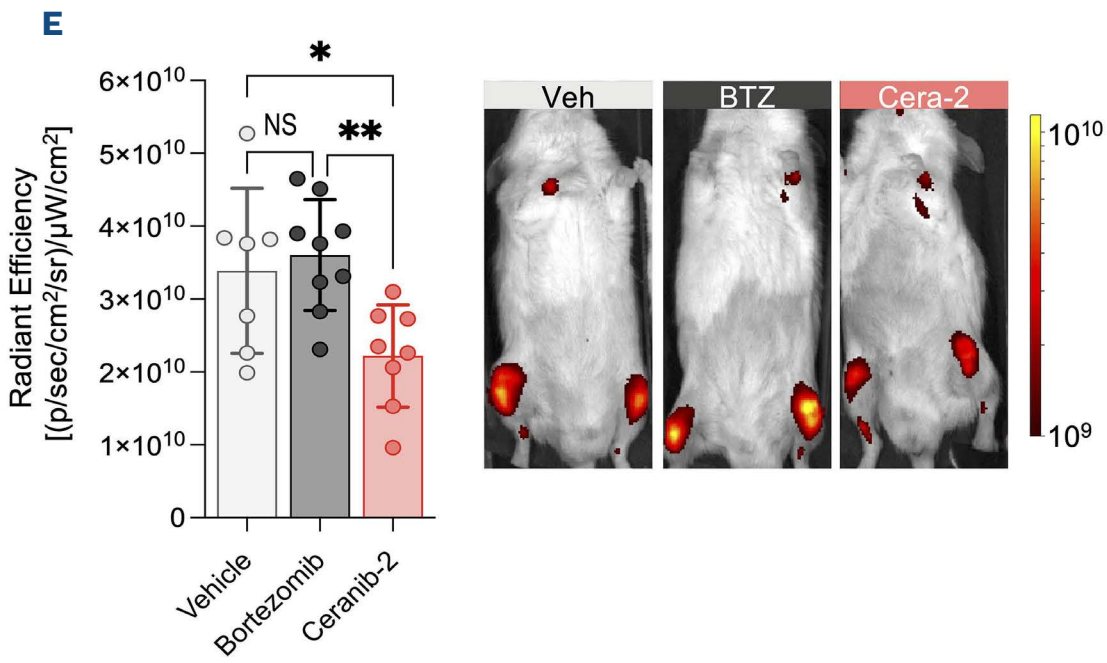

F

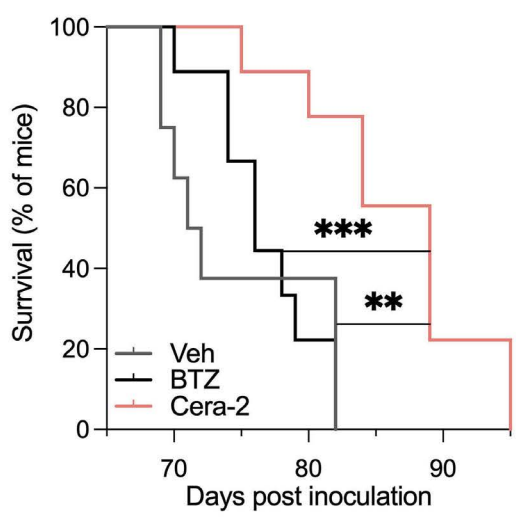

Figure 2. Inhibition of ASAH1 reduces proteasome inhibitor-resistant multiple myeloma cell growth *in vitro* and reduces tumor growth *in vivo*. (A) ASAH1 was knocked down by short hairpin RNA (shRNA) using two independent constructs in PSR multiple myeloma (MM) cells. Control (CTRL) or ASAH1 knockdown (KD1/3) PSR cells were plated in 96-well plates ($0.3x10^6$ cells/mL) and allowed to proliferate. Cell viability was assessed by MTS at the indicated timepoints. Values are mean ± standard deviation (SD) of three independent experiments. (B) A panel of commercial ASAH1 inhibitors was tested on ASAH1 activity (3 hours) and viability (72 hours) in PSR cells, using the ASAH1 activity probe RBM14-C12 and MTS viability assay, respectively. NR: half maximal in-

Continued on following page.

hibitory concentration (IC_{50}) not reached. (C) Sensitive (U266, 8226, ANBL-6, 5TGM1, MM1.S and OPM2) and drug-resistant MM cells (PSR, B25, V10-R, C100R, C300R, DOX6) were plated in 100 μL in 96-well plates ($0.3x10^6$ cells/mL) with increasing concentrations of ceranib-2. Viability was assessed by MTS assay at 72 hours and normalized to that of vehicle-treated controls for each cell line. Box and whisker plots show the calculated IC_{50} values. Each dot represents the average IC_{50} of each cell line. Values are mean ± SD of three independent experiments. (D) NOD.Cg-Prkdc scid Il2rg tm1Wjl /SzJ (NSG) mice were inoculated with PSR-RFP MM cells ($5x10^6$ cells/100 μL) via the tail vein. Tumors were allowed to establish and proliferate for 21 days. Mice were randomized into three groups and treated with ceranib-2 (Cera-2, 5 mg/kg/5 x week, N=8), bortezomib (BTZ, 0.5 mg/kg/2 x week, 72 hours apart, N=9), or vehicle (Veh, N=7) until the end of the study. The line graph shows the total radiant efficiency (as a marker of tumor growth) in mice treated with Cera-2 (N=8), BTZ (N=9), or vehicle (N=7) over the course of the study and prior to the animals reaching study endpoint (hindlimb paralysis or >20% body weight lost) as measured by IVIS Lumina. (E) The bar chart indicates the total radiant efficiency of mice in the Cera-2 (N=8), BTZ (N=9), or vehicle (N=7) treatment groups at the final timepoint in study that included all mice (day 63, left). Representative fluorescence images of red fluorescent protein positive (RFP^+) MM in mice at day 63 (right). (F) The Kaplan-Meier plot shows the percentage of mice treated with Cera-2 (N=8), BTZ (N=9), or vehicle (N=7) reaching endpoint (hindlimb paralysis or >20% body weight lost) over the course of the study. Statistical significance was derived by ordinary one-way analysis of variance (ANOVA) with the Dunnett multiple comparisons test (A, E), Student *t* test (C), two-way ANOVA with Šídák correction (D) and a log-rank (Mantel-Cox) test (F). **P*<0.05, ***P*<0.01, ****P*<0.001, *****P*<0.0001.

in response to PI through degradation of ceramide levels to maintain high levels of active anti-apoptotic proteins.

ASAH1 inhibition restores sensitivity to proteasome inhibitors *in vitro* and *in vivo*

As ASAH1 inhibition reduces both MCL-1 and BCL-2 expression, and given their involvement in PI resistance, we investigated whether ASAH1 inhibition would restore sensitivity to PI treatment. To this end, treatment of control, PI-resistant MM cells with bortezomib had, as expected, no effect on cell viability; however, we noted that $ASAH1^{KD}$ cells were more sensitive to bortezomib treatment at a level that was comparable to their PI-sensitive counterparts (Figure 4A, *Online Supplementary Figure S9A*). Supporting this finding, PI-resistant cells exposed to combination treatment of ceranib-2 and carfilzomib or bortezomib displayed high levels of synergy and MM cell cytotoxicity (Figure 4B, *Online Supplementary Figure S9B*). Next, we asked whether resensitization could be recapitulated *in vivo*. We selected the most efficient shRNA-mediated knockdown (PSR KD1) (*Online Supplementary Figure S4A, B*) for *in vivo* studies. Control or $ASAH1^{KD}$ PSR cells were inoculated into NSG mice and allowed to colonize the skeleton. Once serum IgE levels (a systemic marker of PSR growth) were detected (~ day 21 after inoculation), treatment with bortezomib or vehicle was initiated following clinical dosing and scheduling (twice weekly, 3 days apart) and continued until day 60 (Figure 4C). Only bortezomib-treated $ASAH1^{KD}$ cells exhibited reduced MM growth *in vivo* compared to vehicle-treated control mice, as quantified by serum longitudinal IgE. No significant effects on tumor growth were observed in vehicle-treated $ASAH1^{KD}$ or bortezomib-treated control groups compared to the vehicle-treated control group (Figure 4D). At the study endpoint, we confirmed by flow-cytometry that only bortezomib-treated $ASAH1^{KD}$-treated mice had significantly less (59.89% less) HLA^+ MM cells present in the long bones compared to those in the vehicle-treated control group (Figure 4E). Furthermore, both vehicle- and bortezomib-treated $ASAH1^{KD}$ cells had significantly fewer $MCL\text{-}1^+$ and $BCL\text{-}2^+$ MM cells *ex vivo* compared to vehicle-treated control cells (Figure 4F, *Online Supplementary Figure S9C*). These data further support our findings that inhibition of ASAH1 reduces anti-apoptotic protein expression and restores sensitivity to PI.

Ceramide accumulation inhibits SET resulting in enhanced PP2A activity

Mechanistically, we next interrogated how ASAH1 blockade directly impacted pro-survival protein activity. Of note, the anti-apoptotic activity and stability of MCL-1 and BCL-2 are regulated by phosphorylation events that are governed by numerous kinases and the phosphatase, PP2A. We therefore performed liquid chromatography tandem mass spectrometry proteomics to assess global phosphorylation (STY) changes in wild-type and $ASAH1^{KD}$ MM cells. Robust kinase activity inference (RoKAI) app analysis was used to infer which phosphatases were differentially activated or inhibited (Figure 5A).[35] We noted the activity of PP2A, which dephosphorylates both MCL-1 and BCL-2, increased following ASAH1 inhibition (Figure 5A). We next confirmed our *in-silico* results using a specific PP2A activity assay in which we demonstrated that knockdown of ASAH1 significantly enhanced PP2A activity (Figure 5B). Moreover, we confirmed this observation through treatment with ceranib-2 or via the addition of exogenous ceramide and observed that both approaches induce strong activation of PP2A. Underscoring the specificity of this effect, addition of okadaic acid, a PP2A-specific inhibitor, completely abolished the effects of ASAH1 knockdown, ceranib-2, and ceramide treatment on PP2A activity (Figure 5B).

Previous studies have identified PP2A as a ceramide-activated phosphatase through direct ceramide binding to and inhibition of the endogenous inhibitor SET, also known as I2PP2A.[36,37] While knockdown of ASAH1 had no effect on SET expression (*Online Supplementary Figure S10A*), siRNA-mediated knockdown of SET or pharmacological inhibition with FTY-720[37] reduced both total and phosphorylated MCL-1 and BCL-2 expression (Figure 5C, *Online Supplementary Figure S10B-D*).

Furthermore, knockdown of SET in PI-resistant MM cells

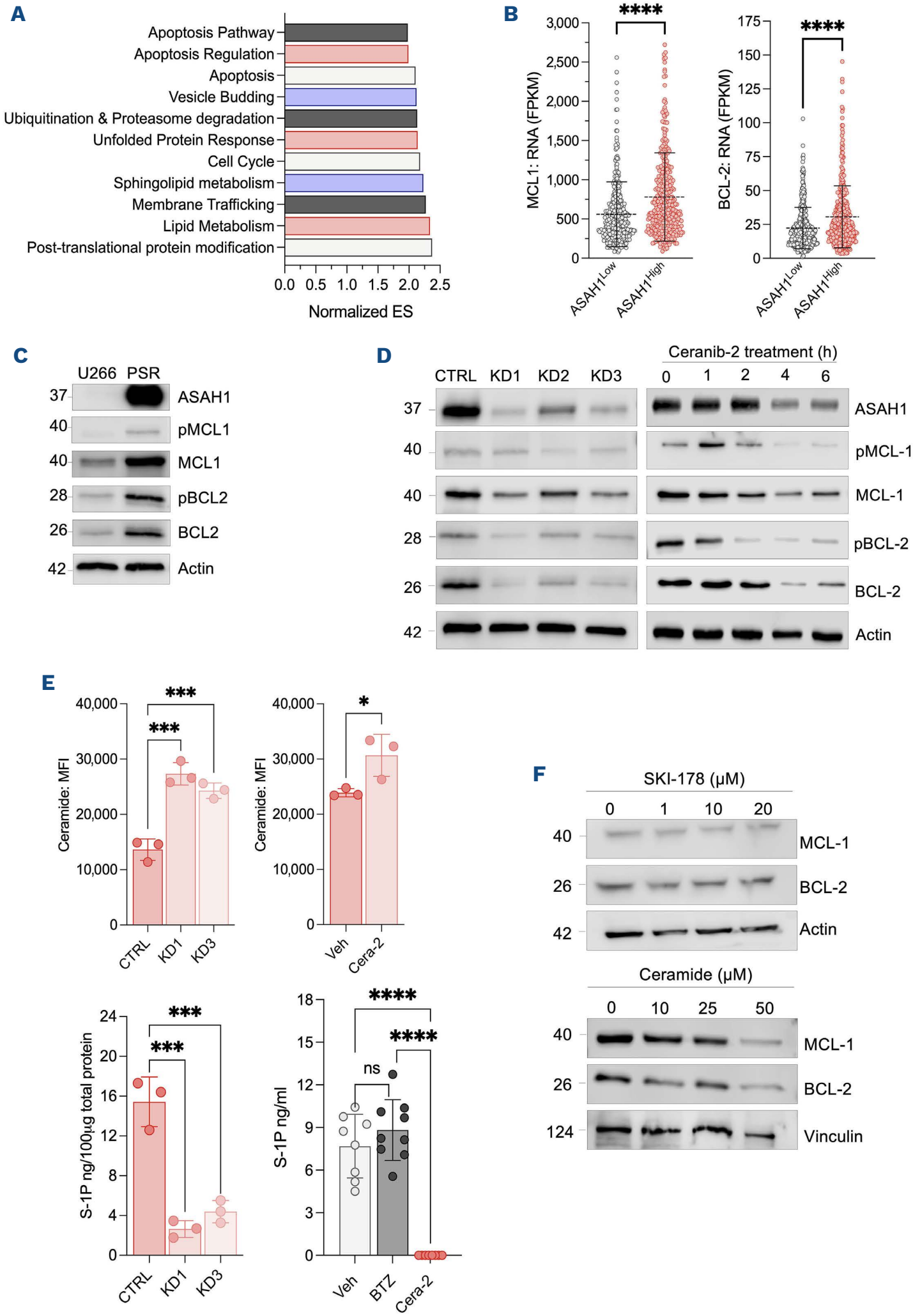

Figure 3. Inhibition of ASAH1 increases ceramide production and reduces S1-P levels, and MCL-1 and BCL-2 phosphorylation and expression in proteasome inhibitor-resistant multiple myeloma. (A) Multiple myeloma (MM) patients from the Multiple Myeloma Research Foundation (MMRF) CoMMpass trial were divided into ASAH1^{Low} (N=385) and ASAH1^{High} (N=385) groups (median split). Gene set analysis was performed on these patients' samples (ASAH1^{High} - ASAH1^{Low}) to determine gene sets that were enriched in patients with elevated ASAH1. The bar chart shows the enriched gene sets in ASAH1^{High} MM patients from the MMRF CoMMpass

Continued on following page.

trial. (B) MM patients from the MMRF CoMMpass trial were divided into ASAH1^{Low} (N=385) and ASAH1^{High} (N=385) groups (median split). The expression of MCL-1 and BCL-2 in each group was assessed. The dot plots show the MCL-1 and BCL-2 gene expression in ASAH1^{Low} (gray, N=385) and ASAH1^{High} (pink, N=385) CoMMpass patients. Each dot represents a patient's sample. (C) Whole cell lysates were prepared from proteasome inhibitor (PI)-sensitive (U266) and PI-resistant (PSR) MM cells. The representative immunoblot shows the expression of ASAH1, pMCL-1 (T163), total MCL-1, p-BCL-2 (S70), total BCL-2 expression and the loading control, actin. Numbers denote the molecular weight (kDa) of each protein. (D) Whole cell lysates were prepared from control (CTRL) or ASAH1 shRNA knockdown (KD1-3) PI-resistant PSR MM cells (left) or PSR cells treated with 2 μM ceranib-2 for the indicated number of hours (right). The representative immunoblot shows the expression of ASAH1, pMCL-1 (T163), total MCL-1, p-BCL-2 (S70), total BCL-2 expression and the loading control actin. (E) Bar charts showing the median fluorescence intensity (MFI) of ceramide levels (top) and sphingosine-1 phosphate (S-1P) levels (bottom) in control (CTRL) or ASAH1 knockdown (KD1-3) PSR cells and PSR cells treated with vehicle or ceranib-2 (2 μM) for 24 hours as assessed by flow cytometry and enzyme-linked immunosorbent assay, respectively. Values are mean ± SD of three independent experiments. (F) Whole cell lysates were prepared from PSR MM cells treated with the indicated concentrations of the sphingosine kinase inhibitor, SKI-178, or ceramide C6 for 4 hours The representative immunoblot shows the expression of total MCL-1, total BCL-2 and the loading controls actin or vinculin. Numbers denote the molecular weight (kDa) of each protein. Statistical significance was derived by an unpaired *t* test (B and E top right panel) and ordinary one-way analysis of variance with the Dunnett multiple comparisons test (E top left and bottom panels). **P*<0.05, ***P*<0.01, ****P*<0.001, *****P*<0.0001.

resensitized these cells to bortezomib treatment, while having no effect on cell viability in the absence of bortezomib (Figure 5D, *Online Supplementary Figure S10E*). These data indicate that ASAH1 promotes high anti-apoptotic protein expression/activity through SET-mediated PP2A inhibition. Of note, in clinical specimens, the expression of ASAH1, SET, MCL1 and BCL2 increased significantly from NDMM to LRMM (Figure 5E). Hierarchical clustering of all 672 PMRC MM samples based on these genes identified three distinct clusters (*Online Supplementary Figure S7D*): cluster 1 (ASAH1/SET/MCL1^{Low} and BCL2^{Med}), cluster 2 (ASAH1/SET/MCL1^{High} and BCL2^{Low}) and cluster 3 (ASAH1/SET/MCL1/BCL2^{High}). RRMM patients belonging to cluster 2 or 3 treated specifically with a PI-containing regimen had significantly shorter overall survival compared to patients belonging to cluster 1 (385 and 583 *vs*. 1,866 days) (*Online Supplementary Figure S11A*) whereas no difference was observed in patients receiving a non-PI-based regimen (*Online Supplementary Figure S11B*). Taken together, these data demonstrate that RRMM cells sustain elevated BCL-2/MCL-1 expression, in part through SET-mediated suppression of PP2A activity. Furthermore, specific inhibition of ASAH1 leads to intracellular ceramide accumulation, in turn activating PP2A and destabilizing MCL-1 and BCL-2 protein expression and activity (Figure 5F).

Ceranib-2 synergizes with carfilzomib to resensitize patient-derived refractory/relapsed multiple myeloma cells *ex vivo*

Thus far, our preliminary data indicated that ASAH1 is a potent mediator of PI resistance in MM. To bolster this finding, we employed the novel *Ex vivo* Mathematical Myeloma Advisor (EMMA) platform.[38,39] This technology allows for the testing of reagents as single therapies, or in combination, on patient-derived CD138^{+} selected MM cells cultured in the presence of patient-derived bone marrow stroma over a 6-day period using live cell imaging (Figure 6A). An area under the curve (AUC) up to 96 hours for each dose was calculated and results are displayed as a mean AUC. Importantly, and in keeping with our earlier findings, ceranib-2 was significantly more effective in targeted killing of cells from patients with RRMM than in those from patients with NDMM (Figure 6B). In fact, ceranib-2 is the only compound for which the AUC was lower in the RRMM group than in the NDMM group (Figure 6C). Given our synergy findings (Figure 4), we next focused on potential synergy within a cohort of NDMM and RRMM patients. We observed that the combination of ceranib-2 and carfilzomib was synergistic in 85.71% of RRMM patients (12/14 synergistic, 1/14 additive and 1/14 antagonistic) and 71.43% of NDMM patients (10/14 synergistic, 4/14 antagonistic) (Figure 6D, E, *Online Supplementary Figure S11C, D*). We also stratified all MM patients by their response to single-agent carfilzomib *ex vivo* (carfilzomib-sensitive: quartile 1; carfilzomib-responsive: quartiles 2 and 3; carfilzomib-resistant: quartile 4). Here, we observed the highest degree of synergy in patients who were carfilzomib-resistant (Figure 6F). Taken together these data indicate that addition of an ASAH1-targeting inhibitor to current PI treatments such as carfilzomib would deepen NDMM patients' responses and resensitize RRMM patients to effective PI treatment.

Discussion

During the course of treatment, the vast majority of MM patients will receive PI-based therapy. While this therapy is initially effective, patients typically become refractory and relapse. Many identified resistance mechanisms in MM converge on the activation of proliferative and anti-apoptotic pathways[13,40,41] and thus targeting of upstream signaling nodes may prove more efficacious. Sphingolipids have long been associated with MM. For example, patients with Gaucher disease have an increased risk of developing MM caused by a deficiency in glucocerebrosidase.[42] Moreover, two of the best characterized sphingolipids, ceramides and S1-P, have been shown to have opposing effects on survival in many healthy and malignant cells.[16] However, the role of sphingolipids and

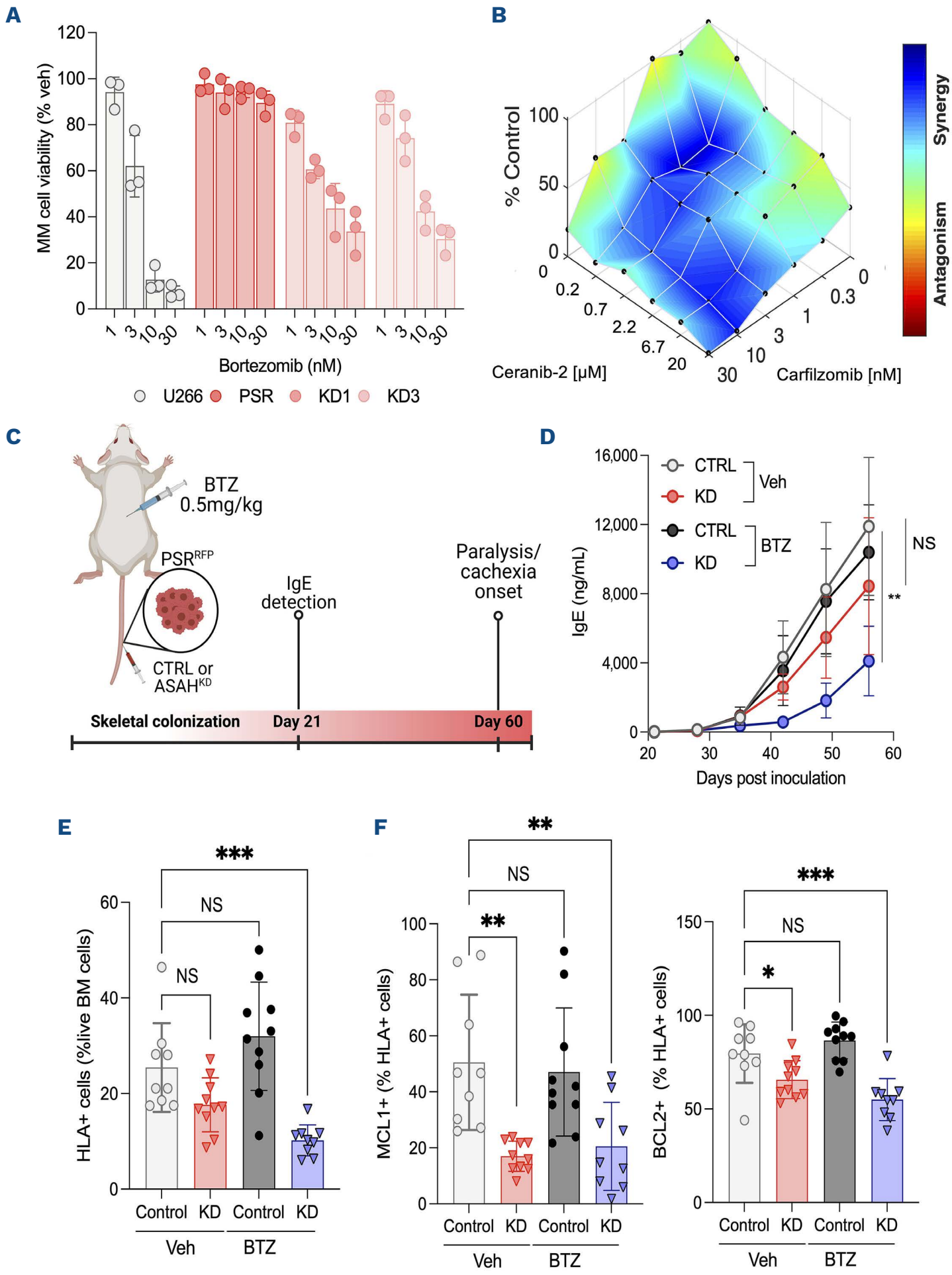

Figure 4. Inhibition of ASAH1 restores sensitivity to proteasome inhibitors in proteasome inhibitor-resistant multiple myeloma cells *in vitro* and *in vivo* through loss of anti-apoptotic proteins. (A) U266, control (CTRL, PSR) and ASAH1 knockdown (PSR KD1/3) MM cells were plated in 100 μL in 96-well plates ($0.3x10^6$ cells/mL) with the indicated concentrations of the proteasome inhibitor (PI), bortezomib (BTZ). Cell viability was assessed at 24 hours by the MTS assay. The bar chart shows the effect of BTZ on U266, CTRL (PSR) and ASAH1 KD (KD1-3) PSR cell viability. Values are mean ± standard deviation (SD) of three independent experiments. (B) PI-resistant PSR MM cells were plated in 100 μL in 96-well plates ($0.3x10^6$ cells/mL) with either vehicle, ceranib-2, carfilzomib or a combination of both drugs at the indicated concentrations for 72 hours. Viability was assessed by an MTS assay, normalized to the vehicle-treated control and LOEWE synergy was calculated using Combenefit. The representative LOEWE synergy plot shows the depth of response (xyz) and the level of antagonism/synergy of ceranib-2 and carfilzomib combinations. Blue

Continued on following page.

areas indicated synergy. (C) Diagram of the *in vivo* study to assess the effect of ASAH1 knockdown on PSR-RFP cell growth. CTRL or ASAH1 knockdown (KD) PSR-RFP cells were injected intravenously. IgE was detected 3 weeks after inoculation. Mice were subdivided into groups and treated with vehicle (Veh), or BTZ (0.5 mg/kg, twice weekly on Mondays and Thursdays). All mice were sacrificed when the first mouse reached study endpoint criteria. (D) Serum was isolated by submandibular bleed and the levels of paraprotein (IgE) were assessed by enzyme-linked immunosorbent assay in CTRL-vehicle (N=9), ASAH1^{KD}-vehicle (N=10) CTRL-BTZ (N=10), ASAH1^{KD}-BTZ (N=9) mice over the course of study. (E) At the study endpoint (the time at which the first mouse developed hindlimb paralysis) all mice were sacrificed and bone marrow cells from the left tibia and femur pair were isolated and subjected to flow cytometry. The bar chart shows the percentage of HLA-A/B/C-positive cells (as a marker of human MM cells) in the bone marrow of CTRL-vehicle (N=9), ASAH1^{KD}-vehicle (N=10) CTRL-BTZ (N=10), ASAH1^{KD}-BTZ (N=9) mice at study endpoint. (F) At the study endpoint (the time at which the first mouse developed hindlimb paralysis) all mice were sacrificed and bone marrow cells from the left tibia and femur pair were isolated and subjected to flow cytometry. The bar chart shows the percentage of MCL-1-positive (left) and BCL-2-positive (right) HLA-A/B/C-positive (MM) cells in the bone marrow of CTRL-vehicle (N=9), ASAH1^{KD}-vehicle (N=10) CTRL-BTZ (N=10), and ASAH1^{KD}-BTZ (N=9) mice. Statistical significance was derived by ordinary one-way analysis of variance with the Dunnett multiple comparisons test (D-F). *P<0.05, **P<0.01, ***P<0.001.

the pathways that control their metabolism have not been investigated in the context of RRMM. Here, we evaluated the expression of sphingolipid metabolism genes in 672 MM patients at different stages of disease and identified acid ceramidase (ASAH1) as being associated with RRMM, specifically in the context of PI-resistance. We then demonstrated that both genetic and pharmacological inhibition of ASAH1 reduces cell viability in models of PI-resistant MM cells *in vitro* and *in vivo*. Excitingly, we also showed that genetic/pharmacological inhibition of ASAH1 renders PI-resistant cells sensitive to PI *in vitro*, *in vivo* and, importantly, in patients' isolated CD138^{+} MM cells *ex vivo*.

Analysis of a sphingolipid metabolism 30-gene signature revealed heightened expression in RRMM *versus* NDMM patients. Of the 12 genes that were significantly upregulated in RRMM, eight controlled ceramide generation. Surprisingly, we found that PI-resistant cell lines had lower levels of total ceramides, but elevated levels of S1-P compared to their drug-sensitive counterparts. In support of this observation, previous studies observed that RRMM patients have reduced levels of ceramides and elevated levels of sphingosine.[17,43] Thus, we focused on the two significantly elevated genes involved in the conversion of ceramide to sphingosine and subsequent phosphorylation to S1-P, i.e., *ASAH1* and *SPHK1*, respectively. Whereas *SPHK1* showed no significant association with any particular treatment regimen, ASAH1 showed significant upregulation in MM patients resistant to any regimen containing a PI. Moreover, patients with elevated levels of ASAH1, regardless of prior therapy, had significantly poorer survival outcomes when treated with any PI-containing regimen but not a non-PI regimen. Recently, it was shown that treatment with bortezomib induces ceramide generation through ceramide synthases and the fatty acid elongase, ELOV6.[43] Thus, elevated ASAH1 may function to break down excess PI-generated ceramides and prevent apoptosis. Interestingly, ASAH1 was also elevated in RRMM patients resistant to anti-CD38 therapies: thus, ASAH1 inhibition may also be beneficial for patients treated with these non-cellular immunotherapies; however, further studies are required to determine whether this is the case, in addition to the precise molecular mechanisms at play.

Using a number of isogenic PI-resistant cell lines we demonstrated that ASAH1 is a therapeutic target for the treatment of PI-resistant MM. Both shRNA and pharmacological inhibition of ASAH1 with ceranib-2 reduced PI-resistant MM growth and resensitized cells to PI through inhibition of the anti-apoptotic proteins MCL-1 and BCL-2 *in vitro* and *in vivo*. Inhibition of ASAH1 also led to an expected increase in total ceramides and a decrease in S1-P levels. Previous studies have shown that targeting S1-P production through inhibition of SPHK1 and 2 reduces the expression of MCL1 but not BCL2 in acute myeloid leukemia and treatment-naïve MM cell lines, respectively.[44-46] SPHK1/2 inhibition in PI-resistant MM did not alter anti-apoptotic protein expression; however, treatment with exogenous ceramide or ceranib-2 led to loss of both proteins and reduced activity (Figure 3). Importantly, ceranib-2, a commercially available ASAH1 inhibitor was effective for the treatment of RRMM *in vivo*, whereas bortezomib was not. While these results are encouraging, previous pharmacokinetic/pharmacodynamic studies have demonstrated that ceranib-2 is rapidly cleared from plasma.[31] Therefore, development of more potent and longer-lasting ceranib-2 derivatives is needed before ASAH1 inhibitors can be translated to the clinic. Collectively, these data further underscore the importance of sphingolipids in different stages of MM and that targeting a key upstream node of sphingolipid metabolism is a relevant therapeutic target for the treatment of RRMM.

While we have focused primarily on the effects of ASAH1 blockade in directly promoting RRMM cell cytotoxicity, we cannot rule out additional effects on the surrounding microenvironment. For example, previous studies demonstrated that alterations in sphingolipids, particularly levels of S1-P, affect angiogenesis and reduce tumor growth *in vivo*.[21,47] While we cannot fully rule out an effect of ceranib-2 on angiogenesis, our *in vivo* models were performed in established RRMM tumors and supported by our *in vitro* data, which point to a MM-specific role of ASAH1 inhibition. Another important caveat is that our *in vivo* studies were performed in immunocompromised mice. NDMM and RRMM patients have demonstrated alterations of immune cells such as expansion of immune suppressive myeloid cells and exhausted γδ T

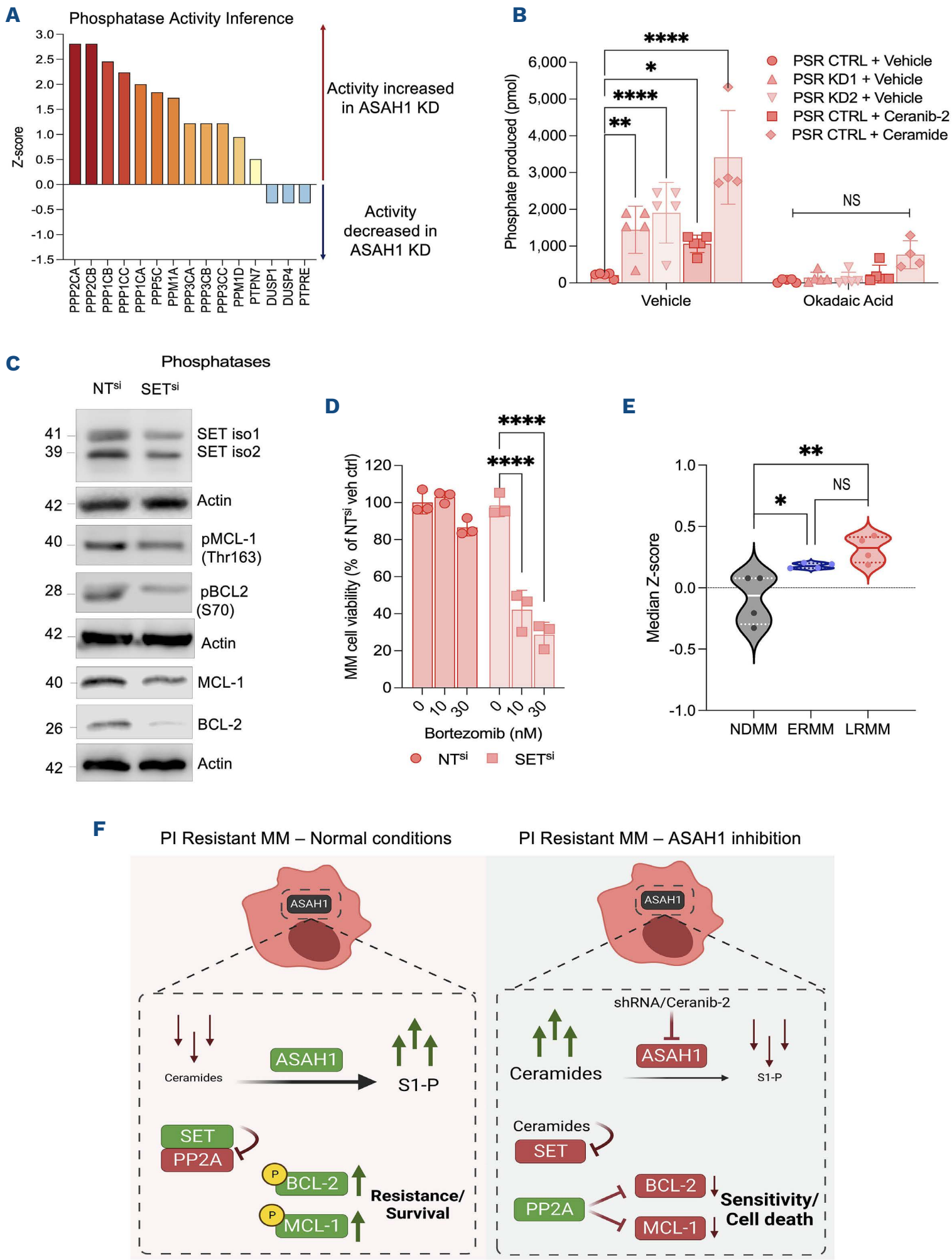

Figure 5. ASAH1 inhibition activates PP2A through ceramide-mediated SET inhibition. (A) Whole cell lysates from control and ASAH1 knockdown (KD) proteosome inhibitor (PI)-resistant multiple myeloma (MM) cells were subject to pSTY phosphoproteomic analysis. Significantly upregulated and downregulated pSTY sites underwent robust inference of kinase activity (RoKAI) analysis to infer changes in phosphatase activity. The bar chart shows the changes in inferred phosphatase activities following ASAH1 knockdown in PI-resistant MM cells (PSR and B25). (B) PP2A activity was assessed in PSR cells following ASAH1 knockdown, or control cells treated with vehicle, ceranib-2 (5 μM) or C6 ceramide (50 μM) for 4 hours, with or without a PP2A-specific inhibitor

Continued on following page.

(okadaic acid, 1 nM). Values are mean ± standard deviation (SD) of four independent experiments. (C) Whole cell lysates were prepared from PSR cells transfected with non-targeting siRNA (NT^{si}) or SET-targeting siRNA (SET^{si}) 48 hours after transfection. The representative immunoblot shows SET isoforms 1 and 2, total and phosphorylated MCL-1, BCL-2 and the loading control, actin, 48 hours after transfection. (D) PI-resistant PSR cells were transfected with NT^{si} or SET^{si}. After 48 hours, cells were plated in 100 μL in 96-well plates ($0.3x10^6$ cells/mL) with the indicated concentrations of bortezomib. After 24 hours (72 hours after transfection) MM cell viability was assessed by MTS assay and viability was normalized to that of vehicle-treated NT^{si} PSR cells. The bar chart shows the effect of SET^{si} alone and in combination with the PI, bortezomib. Values are mean ± SD of three independent experiments. (E) The median expression of SET, ASAH1, MCL-1 and BCL-2 in patients with newly diagnosed MM (NDMM) early resistant/refractory MM (ERMM) and late resistant/refractory (LRMM) patients from the Pentecost Myeloma Research Center RNA-sequencing dataset was assessed. Each dot represents the median expression of a gene in each group of patients. The NDMM, ERMM and LRMM groups contained 187, 303 and 182 patients, respectively. (F) Schematic diagram of PI-resistant MM cells under normal conditions (left) and following ASAH1 inhibition (right). Following ASAH1 inhibition, ceramide levels accumulate and reduce the pool of sphingosine-1 phosphate (S1-P). Ceramide binds to and inhibits SET, thus activating the phosphatase PP2A. PP2A targets BCL-2 and MCL-1 reducing their activity and expression. Reduced levels of anti-apoptotic proteins reduce PI-resistant cell viability and render the cells sensitive to proteasome inhibition and apoptosis. Statistical significance was derived by ordinary one-way analysis of variance with the Dunnett multiple comparisons test (B, D, E). **P*<0.05, ***P*<0.01, ****P*<0.001, *****P*<0.0001.

cells and decreased CD4/CD8 T cells in the bone marrow microenvironment.[48] Thus, a limitation of our study is the lack of syngeneic immunocompetent models as both ceramides and S1-P play roles in the immune system. Recently, it was demonstrated that ceramides/S1-P have opposing roles in the polarization of pro-inflammatory M1 macrophages and anti-inflammatory M2 macrophages, respectively.[47,49] Our data demonstrate that ASAH1 upregulation is also associated with relapse to anti-CD38 therapies, including daratumumab and isatuximab (Figure 1H). ASAH1-mediated degradation of ceramide and subsequent conversion to S1-P in MM cells may push bone marrow macrophages towards an M2-like state. These macrophages are generally believed to be anti-inflammatory, contributing to an immune-suppressed microenvironment and poor response to immunotherapies.[50] Furthermore, accumulation of ceramide synthase-6 generated ceramides in aging T cells was demonstrated to induce mitophagy and limit antitumor immunity.[51] Similarly, S1-P reduces central memory T-cell phenotype, expands immunosuppressive regulatory T cells and diminishes antitumor activity.[52,53] While the role of ASAH1 in individual immune cell subsets is unknown, future studies should further investigate how ASAH1-targeting therapies alter the MM immune microenvironment.

Mechanistically, our studies indicate that ASAH1 blockade leads to ceramide accumulation, which in turn inhibits SET and thus enhances PP2A phosphatase activity. SET has been designated an oncoprotein in several solid and hematologic malignancies via the regulation of histone and non-histone protein acetylation, regulation of the inhibitor of acetyltransferases (INHAT) complex, and the inhibition of the tumor suppressor PP2A.[54-58] Recently, it was discovered that ceramides induce PP2A activation by directly binding to and inhibiting SET.[36,59] PP2A is cellular phosphatase that negatively regulates multiple pro-survival signaling pathways associated with cancer progression such as, ERK, Akt, JAK, β-catenin and c-Myc.[60-63] In drug-naïve MM cell lines, it has been proposed that PP2A increases MCL-1 half-life and that inhibition with okadaic acid results in MM cell death by dephosphorylating Ser159/Thr163 on MCL-1. Our data, however, indicate a role for PP2A-mediated dephosphorylation of MCL-1 Thr163 leading to loss of total protein, thus suggesting that PP2A activation would be an ideal target for the treatment of RRMM. In support of this, it was shown in AML, that pharmacological inhibition of ASAH1 leads to loss of phospho-MCL1 and total MCL-1, but not BCL-2 through an undescribed post-translational mechanism.[34] In addition, we demonstrated that two subgroups of patients with high levels of ASAH1/SET/MCL-1 exist. One subgroup of patients has low levels of BCL-2 and one high. Both of these subgroups have significantly shorter overall survival times compared to ASAH1/SET/$MCL\text{-}1_{Low}$/$BCL\text{-}2_{Med}$ patients. Although this could suggest that BCL-2 expression may not be as important as MCL-1 to MM cell survival, several studies have demonstrated an additive or synergistic benefit of targeting both survival proteins.[64,65] Furthermore, while we have demonstrated a role for ASAH1/SET/PP2A in regulating the expression of anti-apoptotic proteins in RRMM, an alternative explanation is that depletion of ASAH1, rather than restoring sensitivity to PI, activates an alternate pathway leading to apoptosis that is further enhanced by PI. Total protein proteomics revealed changes in the unfolded protein response and endoplasmic reticulum stress upon ASAH1 inhibition (*data not shown*), which are key pathways in MM pathobiology and could explain the enhanced apoptosis observed following ASAH1 inhibition. In other tumor types, ASAH1 expression was shown to alter numerous pathways to drive tumor growth and metastasis, including NFκB, peroxisome biogenesis, and production of reactive oxygen species, neosis and autophagy.[27,34,66-69] Recently, it was shown that elevated ASAH1 levels were correlated with poor response to radiation in patients with prostate cancer. Moreover, the elevated ASAH1 expression was shown to be driven by enhanced activity of the transcription factor, c-Jun in prostate cancer cells. However, the mechanism through which ASAH1 prevents radiation-induced apop-

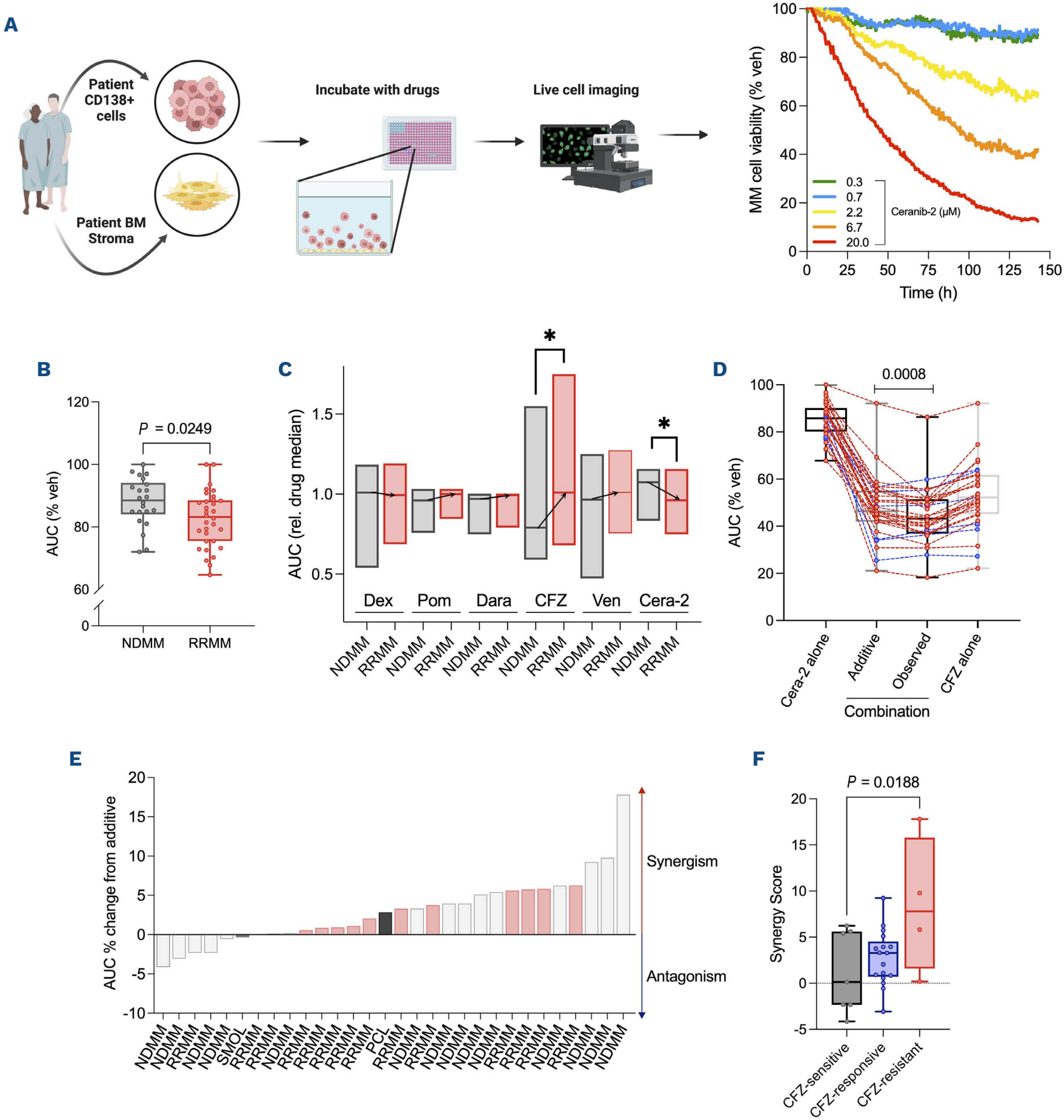

Figure 6. Ceranib-2 synergizes with carfilzomib in most *ex vivo* samples from patients with multiple myeloma. (A) Schematic diagram of the *Ex vivo* Mathematical Myeloma Advisor (EMMA) platform. CD138+ multiple myeloma (MM) cells and bone marrow stroma were isolated from patients and cultured in 384-well plates with drugs for 6 days. Five concentrations of each drug were used. Live cell imaging was used to assess viability over time and median area under the curve (AUC) per patient was calculated at 96 hours. (B) Cells from patients with newly diagnosed MM (NDMM, N=22) and relapsed/refractory MM (RRMM, N=32) were exposed to five concentrations of ceranib-2 in the EMMA platform. The box and whisker plot demonstrates the median AUC for the groups of patients. Each dot represents a different patient. (C) The AUC for different drugs were normalized to the median AUC of each drug. The box plot shows the normalized AUC of the indicated drugs in the NDMM and RRMM patients and only ceranib-2 (Cera-2) was significantly more effective in the RRMM patients. Arrows indicate differences between the patient with NDMM and the patient with RRMM. (D) Thirty patients with plasma cell malignancies (1 smoldering MM [SMOL], 1 plasma cell

Continued on following page.

leukemia [PCL], 14 NDMM, and 14 RRMM patients) were exposed to ceranib-2, carfilzomib or a combination of both drugs in the EMMA platform. The box and whisker plot shows the median AUC of the 30 patients' response *ex vivo* to single-agent ceranib-2 (cera-2), carfilzomib (CFZ), or the combination – either additive or observed. Additive represents the expected value of combining two agents whereas observed indicates the actual response. The difference between additive and observed values was used to calculate either synergy or antagonism. Red dots and lines represent synergy whereas blue lines and dots represent antagonism. (E) The level of synergy or antagonism was assessed in 30 patients treated with ceranib-2 and carfilzomib. The bar chart shows the level of synergy or antagonism (the difference between additive and observed combinations) seen when ceranib-2 and carfilzomib were combined to treat cells *ex vivo* from patient with SMOL (N=1), PCL (N=1), NDMM (N=14), and RRMM (N=14). Positive values indicate synergy whereas negative values indicate antagonism. (F) Box and whisker plot indicating the level of synergy/antagonism in carfilzomib-sensitive (1st quartile, N=7), carfilzomib-responsive (2nd and 3rd quartiles, N=17) and carfilzomib-resistant (4th quartile, N=4) MM patients. Quartiles were identified based on the AUC of carfilzomib responses of 619 MM patients previously tested *ex vivo*. Statistical significance was derived by an unpaired *t* test (B), and ordinary one-way analysis of variance with Šídák correction (C), with the Dunnet correction (D and F). *P<0.05.

tosis was not elucidated. Our study is the first to identify a mechanism through which ASAH1 protects tumor cells against PI-induced apoptosis and the same mechanism may be present in other solid malignancies or in response to other treatments such as anti-CD38 antibodies. While these ASAH1-regulated pathways may also contribute to PI resistance, our data herein show that ASAH1 control of phosphatase PP2A activity is a key mechanism involved in PI-resistance.

In conclusion, we have described a significant and a previously unknown role for ASAH1 in PI-resistance in MM. ASAH1 is not only elevated in PI-resistant MM patients, but its inhibition can also restore PI-sensitivity, through inactivation of SET and reduction of MCL1 and BCL2 expression and activity. These data provide a strong rationale for the development of novel and potent inhibitors of ASAH1 activity, with favorable pharmacokinetic/dynamic profiles, in combination with PI for the treatment of RRMM.

Disclosures

JMK received a salary through a sponsored research agreement with Bristol Myers Squibb (BMS), unrelated to this study. KHS reports having received honoraria from BMS, Janssen, Adaptive, Sanofi, and Takeda, and research funding to his institution from AbbVie and Karyopharm, outside the submitted work. KHS is also a member of advisory boards for Sanofi, GlaxoSmithKline, BMS, Sanofi, Karyopharm, Janssen, and Amgen. The remaining authors have no conflicts of interest to disclose.

Contributions

RTB conceived, designed, performed, analyzed in vitro, in vivo and ex vivo studies, analyzed patients' datasets and wrote the manuscript. TL performed in vitro experiments and assisted with animal studies. RRA analyzed patients' samples and acted as an honest broker for the PMRC MM patient dataset. PRS analyzed and interpreted EMMA platform studies. MMN analyzed patients' data and assisted with animal studies. JSF and NN assisted with animal studies. KJN performed experiments and analyses. MT performed an immunoblotting experiment. BF performed proteomic studies. MBM performed EMMA platform studies. SG provided materials and guidance. ASS conceived and supervised RNA sequencing of clinical samples and EMMA platform analyses. JMK supervised proteomic studies. KHS conceived and supervised studies of patients' samples and EMMA platform studies, and interpreted and provided guidance on clinical data. CCL provided overall supervision and funding, and wrote the manuscript. All authors were involved in reviewing and editing the final manuscript.

Acknowledgments

The authors thank the patients at H. Lee Moffitt Cancer Center who provided clinical samples for our ex vivo assays as well as consented to access to their clinical data through the Total Cancer Care database. The authors also thank the Small Animal Imaging Laboratory, the Flow Cytometry, Tissue, Proteomics and Metabolomics, Biostatistics and Bioinformatics, and Analytical Microscopy Cores of the H. Lee Moffitt Cancer Center and Research Institute, an NCI-designated Comprehensive Cancer Center (P30-CA076292), and the Comparative Medicine Department and the Electron Microscopy Core Facility of the University of South Florida (USF).

Funding

These studies were supported in part by R01-CA239214-01 (to CCL) and R21-CA191981-01A1 (to CCL), Physical Sciences in Oncology grant 1U54CA193489-01A1 (to KHS and ASS), H. Lee Moffitt Cancer Center's Team Science Grant (to AS, KHS), and Miles for Moffitt Foundation (to ASS). Additionally, this work was supported by personal donations from The Pentecost Myeloma Research Center.

Data-sharing statement

All data are available from the corresponding author upon reasonable request. The PI-resistant C300R cells (derived from 5TGM1 murine MM) generated in this study are available from the lead contact (CCL) with a completed Materials Transfer Agreement.

References

1. Kumar SK, Rajkumar V, Kyle RA, et al. Multiple myeloma. Nat Rev Dis Primers. 2017;3:17046.
2. Roodman GD. Pathogenesis of myeloma bone disease. J Cell Biochem. 2010;109(2):283-291.
3. Cowan AJ, Green DJ, Kwok M, et al. Diagnosis and management of multiple myeloma: a review. JAMA. 2022;327(5):464-477.
4. Rajkumar SV, Harousseau JL, Durie B, et al. Consensus recommendations for the uniform reporting of clinical trials: report of the International Myeloma Workshop Consensus Panel 1. Blood. 2011;117(18):4691-4695.
5. Sonneveld P. Management of multiple myeloma in the relapsed/refractory patient. Hematology Am Soc Hematol Educ Program. 2017;2017(1):508-517.
6. Hu J, Hu WX. Targeting signaling pathways in multiple myeloma: pathogenesis and implication for treatments. Cancer Lett. 2018;414:214-221.
7. Jovanovic KK, Roche-Lestienne C, Ghobrial IM, Facon T, Quesnel B, Manier S. Targeting MYC in multiple myeloma. Leukemia. 2018;32(6):1295-1306.
8. Ghermezi M, Spektor TM, Berenson JR. The role of JAK inhibitors in multiple myeloma. Clin Adv Hematol Oncol. 2019;17(9):500-505.
9. Ramakrishnan V, Kumar S. PI3K/AKT/mTOR pathway in multiple myeloma: from basic biology to clinical promise. Leuk Lymphoma. 2018;59(11):2524-2534.
10. Oancea M, Mani A, Hussein MA, Almasan A. Apoptosis of multiple myeloma. Int J Hematol. 2004;80(3):224-231.
11. Inam S, Ross JA, Touzeau C, Moreau P, Kumar SK, Harrison SJ. Paving the way to precision medicine in multiple myeloma. Expert Rev Hematol. 2021;14(4):323-327.
12. Aksoy O, Lind J, Sunder-Plassmann V, Vallet S, Podar K. Bone marrow microenvironment- induced regulation of Bcl-2 family members in multiple myeloma (MM): therapeutic implications. Cytokine. 2023;161:156062.
13. Punnoose EA, Leverson JD, Peale F, et al. Expression profile of BCL-2, BCL-XL, and MCL-1 predicts pharmacological response to the BCL-2 selective antagonist venetoclax in multiple myeloma models. Mol Cancer Ther. 2016;15(5):1132-1144.
14. Evangelisti C, Evangelisti C, Buontempo F, et al. Therapeutic potential of targeting sphingosine kinases and sphingosine 1-phosphate in hematological malignancies. Leukemia. 2016;30(11):2142-2151.
15. Sentelle RD, Senkal CE, Jiang W, et al. Ceramide targets autophagosomes to mitochondria and induces lethal mitophagy. Nat Chem Biol. 2012;8(10):831-838.
16. Young MM, Kester M, Wang HG. Sphingolipids: regulators of crosstalk between apoptosis and autophagy. J Lipid Res. 2013;54(1):5-19.
17. Mohamed A, Collins J, Jiang H, et al. Concurrent lipidomics and proteomics on malignant plasma cells from multiple myeloma patients: probing the lipid metabolome. PLoS One. 2020;15(1):e0227455.
18. Hannun YA, Obeid LM. Sphingolipids and their metabolism in physiology and disease. Nat Rev Mol Cell Biol. 2018;19(3):175-191.
19. Wallington-Beddoe CT PJ, Tong D, Pitson SM, Bradstock KF, Bendall LJ. Sphingosine kinase 2 promotes acute lymphoblastic leukemia by enhancing MYC expression. Cancer Res. 2014;74(10):2803-2815.
20. Liang J, Nagahashi M, Kim EY, et al. Sphingosine-1-phosphate links persistent STAT3 activation, chronic intestinal inflammation, and development of colitis-associated cancer. Cancer Cell. 2013;23(1):107-120.
21. Visentin B, Vekich JA, Sibbald BJ, et al. Validation of an anti-sphingosine-1-phosphate antibody as a potential therapeutic in reducing growth, invasion, and angiogenesis in multiple tumor lineages. Cancer Cell. 2006;9(3):225-238.
22. Zhang L, Liu X, Zuo Z, Hao C, Ma Y. Sphingosine kinase 2 promotes colorectal cancer cell proliferation and invasion by enhancing MYC expression. Tumour Biol. 2016;37(6):8455-8460.
23. Ponnusamy S, Selvam SP, Mehrotra S, et al. Communication between host organism and cancer cells is transduced by systemic sphingosine kinase 1/sphingosine 1-phosphate signalling to regulate tumour metastasis. EMBO Mol Med. 2012;4(8):761-775.
24. Zhuang J, Shirazi F, Singh RK, et al. Ubiquitin-activating enzyme inhibition induces an unfolded protein response and overcomes drug resistance in myeloma. Blood. 2019;133(14):1572-1584.
25. Chen S, Dai Y, Pei XY, et al. CDK inhibitors upregulate BH3-only proteins to sensitize human myeloma cells to BH3 mimetic therapies. Cancer Res. 2012;72(16):4225-4237.
26. Chen S, Zhang Y, Zhou L, et al. A Bim-targeting strategy overcomes adaptive bortezomib resistance in myeloma through a novel link between autophagy and apoptosis. Blood. 2014;124(17):2687-2697.
27. Cheng JC, Bai A, Beckham TH, et al. Radiation-induced acid ceramidase confers prostate cancer resistance and tumor relapse. J Clin Invest. 2013;123(10):4344-4358.
28. Doan NB, Nguyen HS, Montoure A, et al. Acid ceramidase is a novel drug target for pediatric brain tumors. Oncotarget. 2017;8(15):24753-24761.
29. Pizzirani D, Bach A, Realini N, et al. Benzoxazolone carboxamides: potent and systemically active inhibitors of intracellular acid ceramidase. Angew Chem Int Ed Engl. 2015;54(2):485-489.
30. Vethakanraj HS, Sesurajan BP, Padmanaban VP, Jayaprakasam M, Murali S, Sekar AK. Anticancer effect of acid ceramidase inhibitor ceranib-2 in human breast cancer cell lines MCF-7, MDA MB-231 by the activation of SAPK/JNK, p38 MAPK apoptotic pathways, inhibition of the Akt pathway, downregulation of ERalpha. Anticancer Drugs. 2018;29(1):50-60.
31. Draper JM, Xia Z, Smith RA, Zhuang Y, Wang W, Smith CD. Discovery and evaluation of inhibitors of human ceramidase. Mol Cancer Ther. 2011;10(11):2052-2061.
32. Chavez JA, Holland WL, Bar J, Sandhoff K, Summers SA. Acid ceramidase overexpression prevents the inhibitory effects of saturated fatty acids on insulin signaling. J Biol Chem. 2005;280(20):20148-20153.
33. Bedia C, Casas J, Andrieu-Abadie N, Fabrias G, Levade T. Acid ceramidase expression modulates the sensitivity of A375 melanoma cells to dacarbazine. J Biol Chem. 2011;286(32):28200-28209.
34. Tan SF, Liu X, Fox TE, et al. Acid ceramidase is upregulated in AML and represents a novel therapeutic target. Oncotarget. 2016;7(50):83208-83222.
35. Yilmaz S, Ayati M, Schlatzer D, Cicek AE, Chance MR, Koyuturk M. Robust inference of kinase activity using functional networks. Nat Commun. 2021;12(1):1177.
36. De Palma RM, Parnham SR, Li Y, et al. The NMR-based characterization of the FTY720-SET complex reveals an alternative mechanism for the attenuation of the inhibitory

SET-PP2A interaction. FASEB J. 2019;33(6):7647-7666.
37. Saddoughi SA, Gencer S, Peterson YK, et al. Sphingosine analogue drug FTY720 targets I2PP2A/SET and mediates lung tumour suppression via activation of PP2A-RIPK1-dependent necroptosis. EMBO Mol Med. 2013;5(1):105-121.
38. Silva A, Silva MC, Sudalagunta P, et al. An ex vivo platform for the prediction of clinical response in multiple myeloma. Cancer Res. 2017;77(12):3336-3351.
39. Sudalagunta P, Silva MC, Canevarolo RR, et al. A pharmacodynamic model of clinical synergy in multiple myeloma. EBioMedicine. 2020;54:102716.
40. Abdi J, Chen G, Chang H. Drug resistance in multiple myeloma: latest findings and new concepts on molecular mechanisms. Oncotarget. 2013;4(12):2186-2207.
41. Seiller C, Maiga S, Touzeau C, et al. Dual targeting of BCL2 and MCL1 rescues myeloma cells resistant to BCL2 and MCL1 inhibitors associated with the formation of BAX/BAK hetero-complexes. Cell Death Dis. 2020;11(5):316.
42. Barth BM, Shanmugavelandy SS, Tacelosky DM, Kester M, Morad SA, Cabot MC. Gaucher's disease and cancer: a sphingolipid perspective. Crit Rev Oncog. 2013;18(3):221-234.
43. Lipchick BC, Utley A, Han Z, et al. The fatty acid elongase ELOVL6 regulates bortezomib resistance in multiple myeloma. Blood Adv. 2021;5(7):1933-1946.
44. Hengst JA, Dick TE, Sharma A, et al. SKI-178: a multitargeted inhibitor of sphingosine kinase and microtubule dynamics demonstrating therapeutic efficacy in acute myeloid leukemia models. Cancer Transl Med. 2017;3(4):109-121.
45. Venkata JK, An N, Stuart R, et al. Inhibition of sphingosine kinase 2 downregulates the expression of c-Myc and Mcl-1 and induces apoptosis in multiple myeloma. Blood. 2014;124(12):1915-1925.
46. Powell JA, Lewis AC, Zhu W, et al. Targeting sphingosine kinase 1 induces MCL1-dependent cell death in acute myeloid leukemia. Blood. 2017;129(6):771-782.
47. Weigert A, Tzieply N, von Knethen A, et al. Tumor cell apoptosis polarizes macrophages role of sphingosine-1-phosphate. Mol Biol Cell. 2007;18(10):3810-3819.
48. Yao L, Jayasinghe RG, Lee Bh, et al. Comprehensive characterization of the multiple myeloma immune microenvironment using integrated scRNA-seq, CyTOF, and CITE-seq analysis. Cancer Res Commun. 2022;2(10):1255-1265.
49. Sun H, Sun S, Chen G, et al. Ceramides and sphingosine-1-phosphate mediate the distinct effects of M1/M2-macrophage infusion on liver recovery after hepatectomy. Cell Death Dis. 2021;12(4):324.
50. Usmani SZ, Khan I, Chiu C, et al. Deep sustained response to daratumumab monotherapy associated with T-cell expansion in triple refractory myeloma. Exp Hematol Oncol. 2018;7:3.
51. Vaena S, Chakraborty P, Lee HG, et al. Aging-dependent mitochondrial dysfunction mediated by ceramide signaling inhibits antitumor T cell response. Cell Rep. 2021;35(5):109076.
52. Priceman SJ, Shen S, Wang L, et al. S1PR1 is crucial for accumulation of regulatory T cells in tumors via STAT3. Cell Rep. 2014;6(6):992-999.
53. Chakraborty P, Vaena SG, Thyagarajan K, et al. Pro-survival lipid sphingosine-1-phosphate metabolically programs T cells to limit anti-tumor activity. Cell Rep. 2019;28(7):1879-1893.e7.
54. von Lindern M, van Baal S, Wiegant J, Raap A, Hagemeijer A, Grosveld G. Can, a putative oncogene associated with myeloid leukemogenesis, may be activated by fusion of its 3' half to different genes: characterization of the set gene. Mol Cell Biol. 1992;12(8):3346-3355.
55. Adachi Y, Pavlakis GN, Copeland TD. Identification and characterization of SET, a nuclear phosphoprotein encoded by the translocation break point in acute undifferentiated leukemia. J Biol Chem. 1994;269(3):2258-2262.
56. Di Mambro A, Esposito MT. Thirty years of SET/TAF1beta/I2PP2A: from the identification of the biological functions to its implications in cancer and Alzheimer's disease. Biosci Rep. 2022;42(11):BSR20221280.
57. Seo SB, McNamara P, Heo S, Turner A, Lane WS, Chakravarti D. Regulation of histone acetylation and transcription by INHAT, a human cellular complex containing the set oncoprotein. Cell. 2001;104(1):119-130.
58. Seo SB, Macfarlan T, McNamara P, et al. Regulation of histone acetylation and transcription by nuclear protein pp32, a subunit of the INHAT complex. J Biol Chem. 2002;277(16):14005-14010.
59. Mukhopadhyay A, Saddoughi SA, Song P, et al. Direct interaction between the inhibitor 2 and ceramide via sphingolipid-protein binding is involved in the regulation of protein phosphatase 2A activity and signaling. FASEB J. 2009;23(3):751-763.
60. Arnold HK, Sears RC. A tumor suppressor role for PP2A-B56alpha through negative regulation of c-Myc and other key oncoproteins. Cancer Metastasis Rev. 2008;27(2):147-158.
61. Gotz J, Probst A, Mistl C, Nitsch RM, Ehler E. Distinct role of protein phosphatase 2A subunit Calpha in the regulation of E-cadherin and beta-catenin during development. Mech Dev. 2000;93(1-2):83-93.
62. Samanta AK, Chakraborty SN, Wang Y, et al. Jak2 inhibition deactivates Lyn kinase through the SET-PP2A-SHP1 pathway, causing apoptosis in drug-resistant cells from chronic myelogenous leukemia patients. Oncogene. 2009;28(14):1669-1681.
63. Resjo S, Goransson O, Harndahl L, Zolnierowicz S, Manganiello V, Degerman E. Protein phosphatase 2A is the main phosphatase involved in the regulation of protein kinase B in rat adipocytes. Cell Signal. 2002;14(3):231-238.
64. Carter BZ, Mak PY, Tao W, et al. Maximal activation of apoptosis signaling by cotargeting antiapoptotic proteins in BH3 mimetic-resistant AML and AML stem cells. Mol Cancer Ther. 2022;21(6):879-889.
65. Yi X, Sarkar A, Kismali G, et al. AMG-176, an Mcl-1 antagonist, shows preclinical efficacy in chronic lymphocytic leukemia. Clin Cancer Res. 2020;26(14):3856-3867.
66. Tan SF, Dunton W, Liu X, et al. Acid ceramidase promotes drug resistance in acute myeloid leukemia through NF-kappaB-dependent P-glycoprotein upregulation. J Lipid Res. 2019;60(6):1078-1086.
67. White-Gilbertson S, Lu P, Norris JS, Voelkel-Johnson C. Genetic and pharmacological inhibition of acid ceramidase prevents asymmetric cell division by neosis. J Lipid Res. 2019;60(7):1225-1235.
68. Lai M, Amato R, La Rocca V, et al. Acid ceramidase controls apoptosis and increases autophagy in human melanoma cells treated with doxorubicin. Sci Rep. 2021;11(1):11221.
69. Malvi P, Janostiak R, Nagarajan A, Zhang X, Wajapeyee N. N-acylsphingosine amidohydrolase 1 promotes melanoma growth and metastasis by suppressing peroxisome biogenesis-induced ROS production. Mol Metab. 2021;48:101217.